Am J Transl Res 2022;14(11):7653-7669
www.ajtr.org /ISSN:1943-8141/AJTR0144975

*Original Article*

# m$^6$A-related lncRNA signature for predicting prognosis and immune response in head and neck squamous cell carcinoma

Ji Yin*, Xinling He*, Fengfeng Qin, Sihan Zheng, Yanlin Huang, Lanxin Hu, Yuxiang Chen, Lunkun Zhong, Wenjian Hu, Sen Li

*The Affiliated Traditional Chinese Medicine Hospital of Southwest Medical University, Luzhou 646000, Sichuan, China. *Equal contributors.*

Received June 27, 2022; Accepted September 27, 2022; Epub November 15, 2022; Published November 30, 2022

**Abstract:** Objectives: N6-methyladenosine (m$^6$A) and long non-coding RNAs (lncRNAs) significantly impact the prognosis and the response to immunotherapy in head and neck squamous cell carcinoma (HNSCC). Therefore, this study aimed to develop an m$^6$A-related lncRNA (m$^6$AlncRNA) model for predicting the prognosis and the immunotherapeutic response in HNSCC. Methods: We identified the m$^6$AlncRNAs and constructed a risk assessment signature by using univariable Cox, Least Absolute Shrinkage and Selection Operator (LASSO), and multivariate Cox regression analyses. The Kaplan-Meier analysis, receiver-operating characteristic (ROC) curves, principal component analysis (PCA), decision curve analysis (DCA), consistency index (C-index), and nomogram were applied to assess the risk model. Finally, we investigated the predictability of this model in prognosis and response to immunotherapy and evaluated various novel compounds for the clinical treatment of HNSCC. Results: HNSCC patients were assigned to high- and low-risk groups based on the median risk scores, and the high- and low-risk groups had different clinical features, tumor immune infiltration status, tumor immune dysfunction and exclusion (TIDE), tumor mutational burden (TMB), sensitivity to novel potential compounds, and immunotherapeutic response. Conclusions: The model we developed was accurate and efficient in predicting the prognosis of patients with HNSCC. It was also sensitive in stratifying HNSCC patients with good response to immunotherapy. Therefore, our study provided insight into elucidating the processes and mechanisms of m$^6$AlncRNAs.

**Keywords:** Head and neck squamous cell carcinoma, N6-methyladenosine, long non-coding RNAs, immune, prognostic model, bioinformation analysis

## Introduction

Head and neck squamous cell carcinoma (HNSCC) is a prevalent cancer worldwide, leading to around 350,000 deaths every year [1, 2]. Although in the past few decades, the standard treatment for HNSCC has greatly improved [3], the five-year survival rate of HNSCC patients is still only about 50% [4]. Emerging evidence indicates that the identification and application of molecular biomarkers could offer prognostic benefit to HNCSCC patients [5].

The most common RNA modification in eukaryotes is N6-methyladenosine (m$^6$A), which influences virtually every aspect of mRNA metabolism [5]. The dynamic interaction among methyltransferases, or "writers", demethylases, or "erasers", and signal transducers, or "readers", mediates the regulatory effects of this modification [7]. Furthermore, m$^6$A is known as the most common and abundant internal alteration found in long non-coding RNAs (lncRNAs) and mRNAs [7], and m$^6$A-regulated lncRNAs modulate the initiation and progression of HNSCC. For example, LNCAROD is stabilized by m$^6$A methylation mediated by METTL3 and METTL14, which contributes to the progression of HNSCC by formulating ternary complexes [9]. In another study, Li et al. reported that ALKBH5-regulated m$^6$A modification of KCNQ1OT1 promoted the progress of HNSCC by up-regulating HOXA9 [10]. Nevertheless, the detailed mechanisms underlying the regulation of m$^6$A in lncRNAs remain to be fully elucidated.

In this study, we first identified the m6AlncRNAs and constructed a risk assessment signature by using univariable Cox, Least Absolute Shrinkage and Selection Operator (LASSO), and multivariate Cox regression analyses. Then, we investigated the immunological characteristics and the response to immunotherapy of different risk groups stratified by this model and evaluated various novel compounds for the clinical treatment of HNSCC. In conclusion, we have developed a prognostic risk model for HNSCC based on m6AlncRNAs that could predict the prognosis and the response to immunotherapy in HNSCC.

## Materials and methods

### *Data collection*

RNA-seq data, clinical information, and gene mutation data of HNSCC were downloaded from The Cancer Genome Atlas (TCGA, https://tcga-data.nci.nih.gov/tcga). Duplicate data or those with incomplete clinical information such as missing patient follow-up were excluded. The expression profiles of mRNAs and lncRNAs were extracted by adding annotations based on the Ensembl database (http://asia.ensembl.org). A total of 23 m6A genes were obtained based on the information from previous stu dies (Table S1). The R package limma was further used to identify m6AlncRNAs based on the standard cor > 0.4 and P < 0.001 (Table S2). The m6A-transcriptome profile of HSNCC patients was investigated in this study.

### *Development of risk assessment model*

The entire TCGA set was randomly divided into training and validation sets. The prognostic value of m6AlncRNAs was first evaluated by univariate Cox analysis in the training set (P < 0.05). LASSO analysis was then applied to further screen m6AlncRNAs, and finally multivariate Cox analysis was employed to establish a prognostic risk model. The risk scores for all patients were computed according to the following formula: $\sum_{i=1}^{k} \beta i Si$. Based on the median risk score derived from the above formula, we assigned the patients into high- and low-risk groups.

### *Validation of the prognostic risk model*

The Kaplan-Meier analysis was applied to assess the difference in survival between the high- and low-risk groups. The time-dependent receiver-operating characteristic (ROC) curves and the area under the curve (AUC) were applied to estimate the predictive ability of the signature for survival compared to the traditional clinical features and the established models [11-14]. We further compared the difference in survival between these two groups in subgroups defined by clinicopathological characteristics. Principal component analysis (PCA) analysis was performed for the exploratory visualization of the high-dimensional data of the whole gene expression landscape, m6A genes, m6AlncRNAs, and the m6AlncRNAs in the model. Moreover, to validate the model as an independent prognostic predictor, we applied univariate and multivariate Cox analyses. We also employed decision curve analysis (DCA) and consistency index (C-index) to evaluate the accuracy of the model compared to the traditional clinical features. A nomogram integrating prognostic signatures was constructed to predict 1-, 3-, and 5-year survival rates of patients.

### *Exploration of immunological atlas*

To obtain a reliable immune infiltration status, various currently accepted methods were employed, including XCELL, TIMER, QUANTISEQ, MCPCOUNTER, EPIC, CIBERSORT-ABS, and CIBERSORT. The single-sample gene set enrichment analysis (ssGSEA) was performed to investigate the difference in immune function between the high- and low-risk groups. The expression levels of the immune checkpoint inhibitors (ICIs)-related genes between these two groups were studied using Wilcoxon signed rank test. The gene mutation analysis was applied to ascertain the quantity and quality of gene mutations between these two groups. The tumor mutational burden (TMB) and tumor immune dysfunction and exclusion (TIDE) were employed to predict the difference in immunotherapeutic response among different risk groups.

### *Identification of potential compounds*

To identify potential compounds for HNSCC treatment, we computed the half inhibitory concentration (IC50) of compounds and compared the difference in the IC50 between high- and low-risk groups.

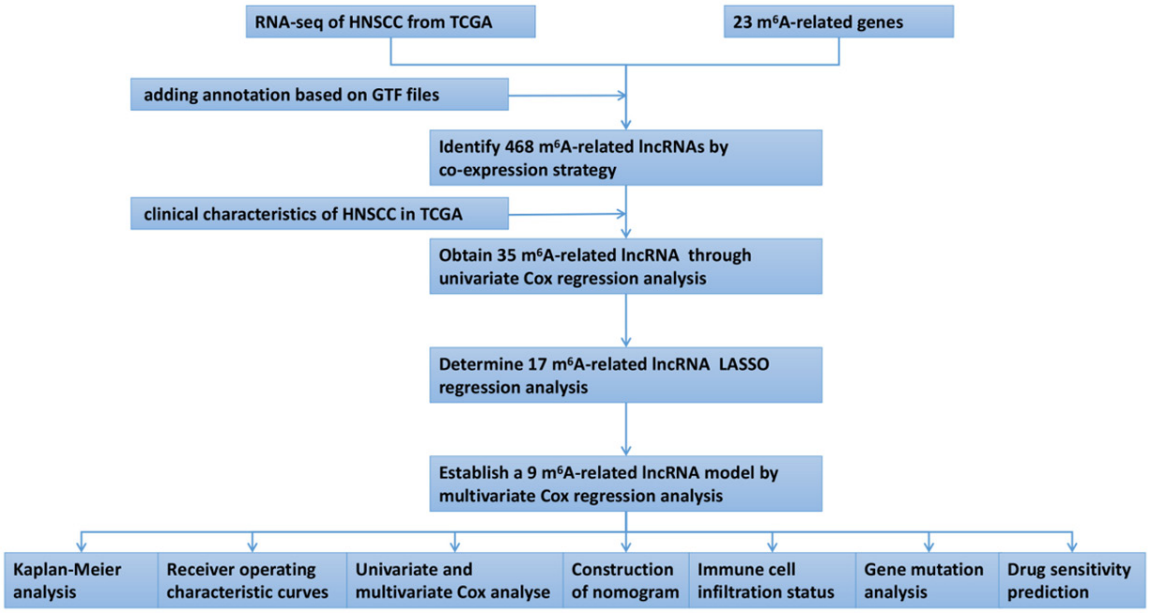


**Figure 1.** Flowchart of the study.

## Results

### *Identification of m$^6$AlncRNAs*

The flowchart representing the procedure of this study was summarized in **Figure 1**. The RNA-seq data, clinical information, and gene mutation data of HNSCC were first collected in TCGA, including 498 tumor and 44 normal samples. Then, 14,086 lncRNAs were retrieved based on the above data. Finally, 468 m$^6$AlncRNAs were identified by co-expression analysis (cor > 0.4 and P < 0.001). The co-expression network was visualized in **Figure 2A**, and the association of m$^6$A genes with m$^6$AlncRNAs was shown in **Figure 2B**.

### *Development of prognostic risk model*

The entire TCGA set (498 tumor samples) was randomly assigned to training (350 samples) and validation sets (148 samples) as a 7-to-3 ratio, and a prognostic risk model was developed. Univariate Cox analysis was then utilized to select 35 m$^6$AlncRNAs with potential prognostic value from the 468 m$^6$AlncRNAs identified above (P < 0.05, **Figure 3A**). Next, the LASSO analysis was employed to filter out 17 candidate m$^6$AlncRNAs among these 35 prognostic m$^6$AlncRNAs (**Figure 3B** and **3C**). Finally, a risk assessment model was established by using multivariate Cox analysis, which included 9 m$^6$AlncRNAs (SNHG16, JPX, AL450384.2, AL157932.1, AC002310.1, AC010226.1, DTX2-P1-UPK3BP1-PMS2P11, AC106820.5, and AL513190.1) (**Figure 3D**). Based on the median risk score, out of the 498 tumor samples used, 244 samples were assigned to the high-risk group, while 254 samples to the low-risk group.

### *Verification of the risk assessment model*

**Figure 3** showed the results of the survival analysis, the expression profiles of the m$^6$AlncRNAs, the pattern of survival status, and the distribution of risk grades between the high- and low-risk groups in the training set (**Figure 4A-D**), in the validation set (**Figure 4E-H**), and in the entire set (**Figure 4I-L**). All these analyses suggested that the patients in the high-risk group had a shorter survival time. Furthermore, the ROC curves indicated the high sensitivity and specificity in survival prediction of our signature, with the 5-year AUC value was 0.774 in the training set (**Figure 5A**), 0.740 in the validation set (**Figure 5B**), and 0.731 in the entire set (**Figure 5C**). Moreover, the 5-year AUC value of the signature was higher than the traditional clinical features and the published models (**Figures 5A** and S1).

Importantly, even in the subgroups defined by age, gender, pathological stage, and T stage, the patients in the low-risk subgroup had longer survival times compared to the patients in the high-risk subgroup, demonstrating that our

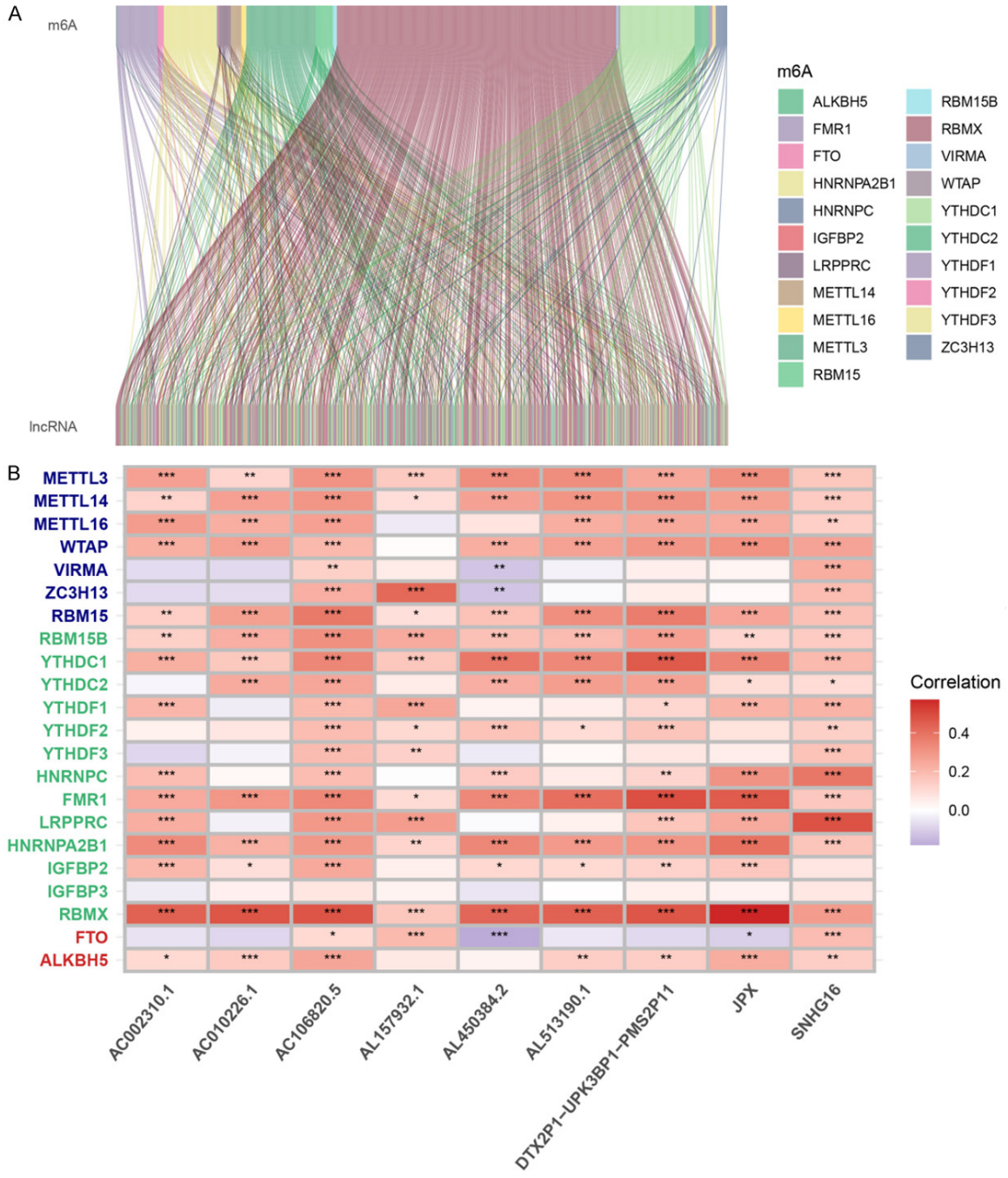


**Figure 2.** A. Sankey diagram for the co-expression correlations between 23 N6-methyladenosine ($m^6A$) genes and $m^6A$-related long non-coding RNAs ($m^6A$lncRNAs). B. Heatmap for the co-expression correlations between 23 $m^6A$ genes and the 9 $m^6A$lncRNAs used to construct the model. *, P < 0.05; **, P < 0.01; ***, P < 0.001.

model was applicable to various circumstances (**Figure 6A**). PCA indicated that the distributions of whole gene expression profiles, the 23 $m^6A$ genes, and the $m^6A$lncRNAs between the high- and low-risk groups were relatively scattered (**Figure 6B-D**), while the distributions of the nine $m^6A$lncRNAs in the signature had different distributions (**Figure 6E**).

Furthermore, univariate Cox analysis demonstrated that the risk score was statistically related to prognosis (P < 0.001; **Figure 7A**), and multivariate Cox analysis demonstrated that the risk score was an independent prognostic risk factor (P < 0.001; **Figure 7B**). The C-index and DCA demonstrated that our signature performed better in predicting the prognosis of

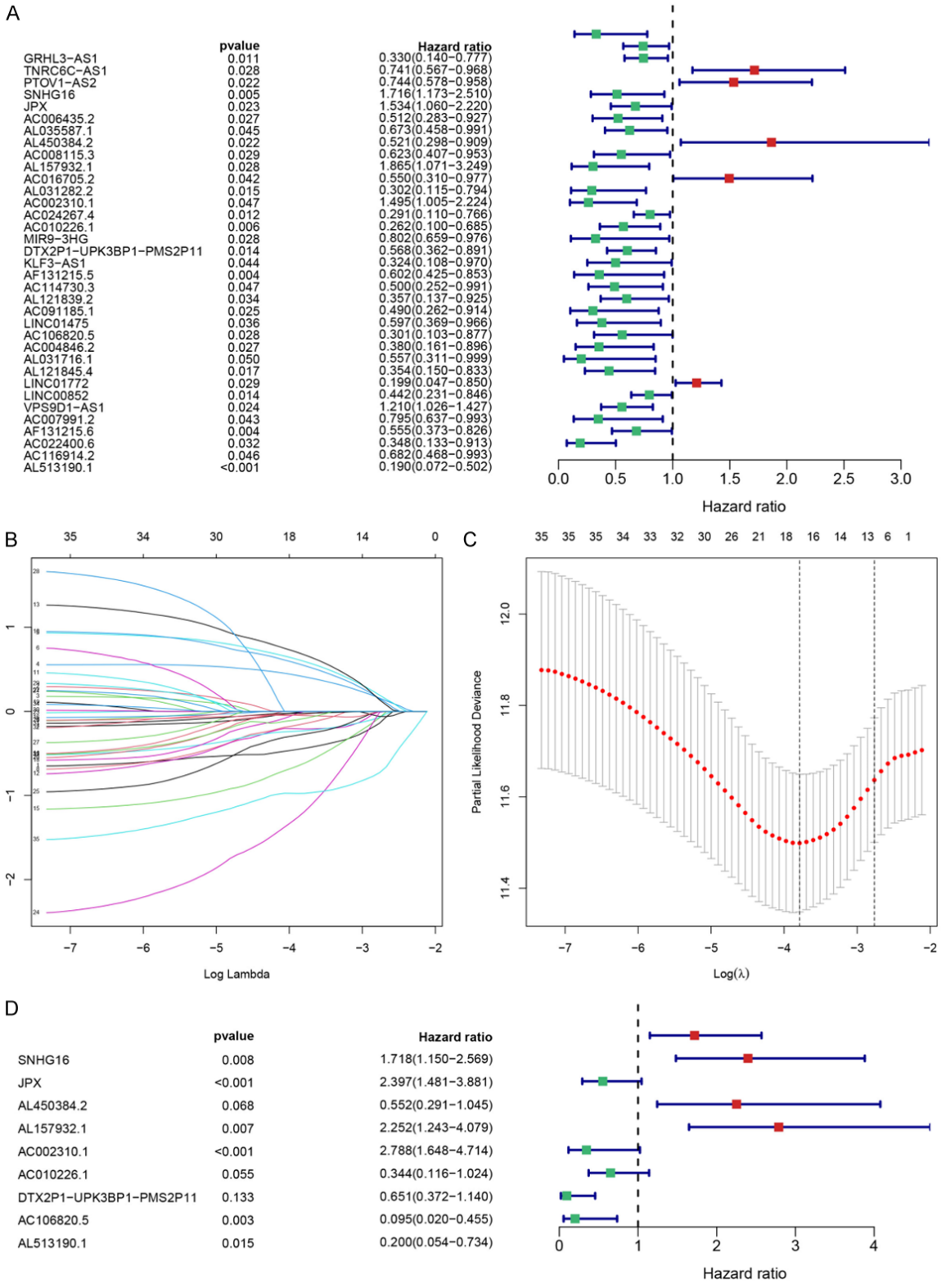


**Figure 3.** A. 35 prognostic m$^6$AlncRNAs recognized by univariate Cox analysis. B. Least Absolute Shrinkage and Selection Operator (LASSO) coefficient profiles of the prognostic m$^6$AlncRNAs. C. Coefficient profile plot generated against the log sequence. D. 9 m$^6$AlncRNAs identified by multivariate Cox regression analysis.

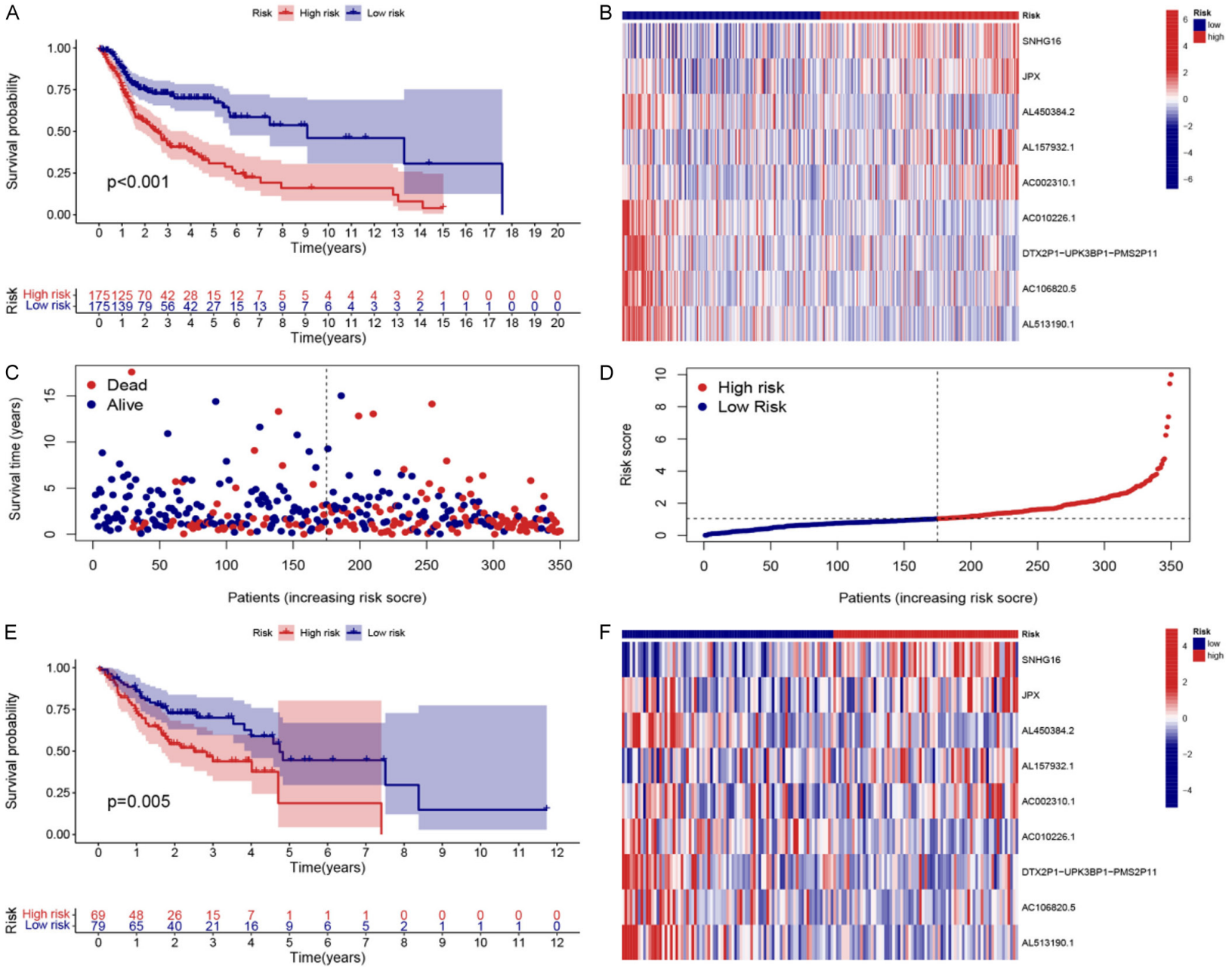
A
Risk
High risk
Low risk
Survival probability
p<0.001
Time(years)
High risk
Low risk
B
Risk
SNHG16
JPX
AL450384.2
AL157932.1
AC002310.1
AC010226.1
DTX2P1-UPK3BP1-PMS2P11
AC106820.5
AL513190.1
low
high
C
Dead
Alive
Survival time (years)
Patients (increasing risk socre)
D
High risk
Low Risk
Risk score
Patients (increasing risk socre)
E
Risk
High risk
Low risk
Survival probability
p=0.005
Time(years)
High risk
Low risk
F
Risk
SNHG16
JPX
AL450384.2
AL157932.1
AC002310.1
AC010226.1
DTX2P1-UPK3BP1-PMS2P11
AC106820.5
AL513190.1
low
high

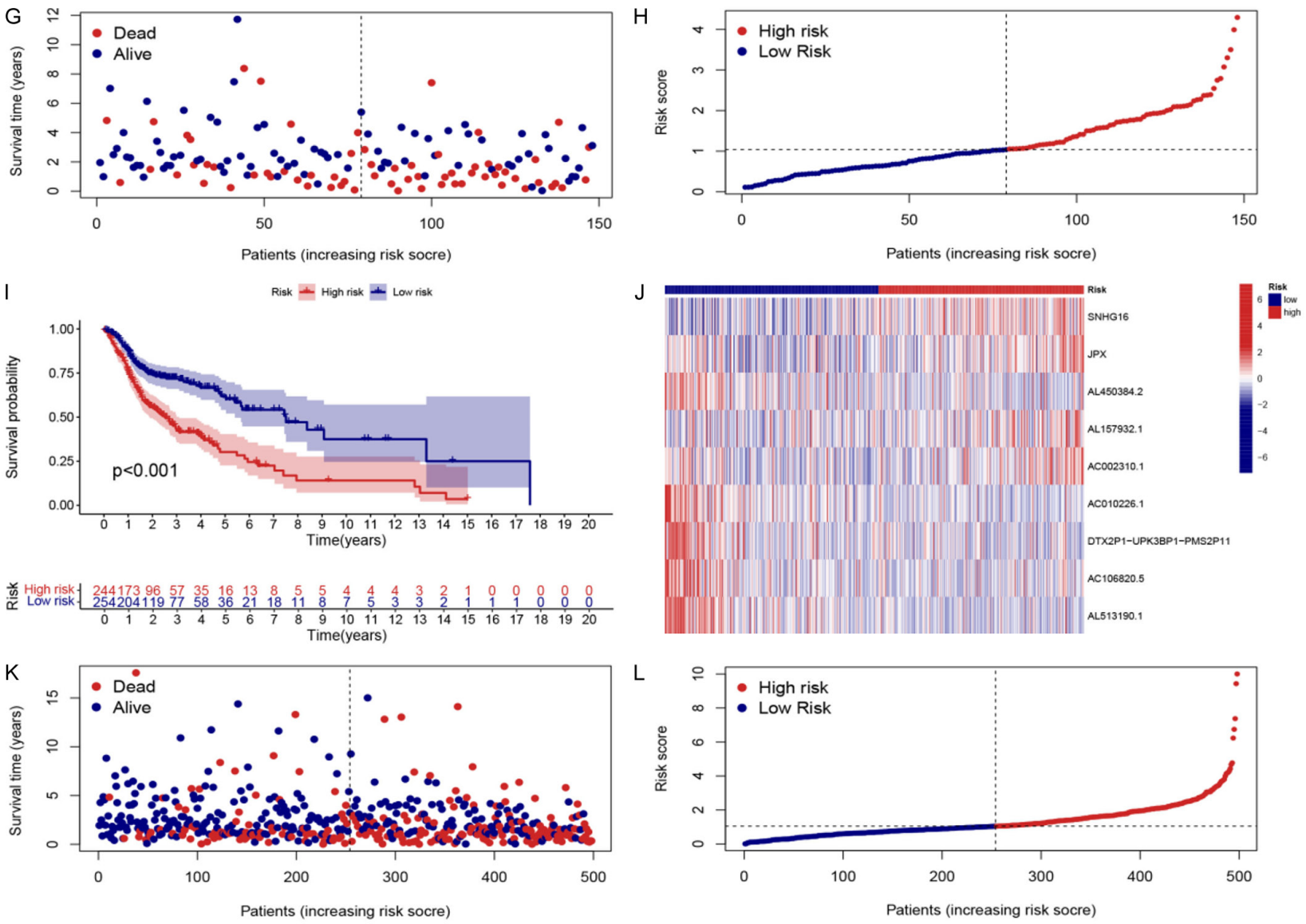


**Figure 4.** Kaplan-Meier survival curve of the expression of the 9 prognostic m$^6$AlncRNAs (A), the patterns of survival outcome (B), and the distribution of risk score (C) for patients between different groups in the training set (D). Kaplan-Meier survival curve of the expression of the 9 prognostic m$^6$AlncRNAs (E), the patterns of survival outcome (F), and the distribution of risk score (G) for patients between diverse groups in the validation set (H). Kaplan-Meier survival curve of the expression of the 9 prognostic m$^6$AlncRNAs (I), the patterns of survival outcome (J), and the distribution of risk score (K) for patients between diverse groups in the entire set (L).

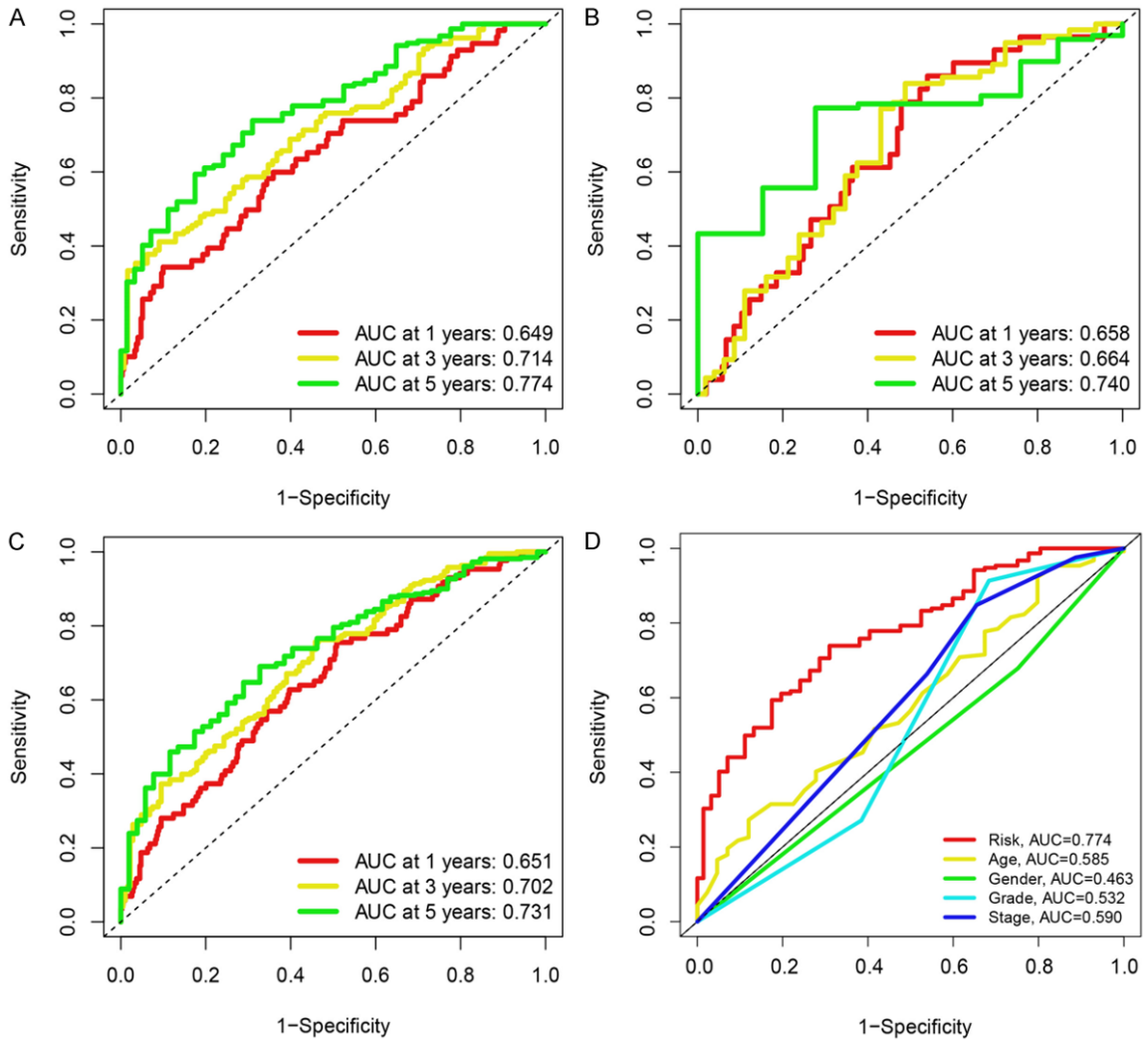


**Figure 5.** A-C. The 5-year time-dependent receiver-operating characteristic (ROC) curves demonstrated the high sensitivity and specificity of the model for survival prediction, and the area under curve (AUC) value was 0.774 in the training set, 0.740 in the testing set, and 0.731 in the entire set. D. A comparison of 5-year ROC curves with the traditional clinical features indicated the superiority of this risk model.

HNSCC than other traditional clinical features (**Figure 7C**, **7D**). The nomogram that integrated the signature and clinical features was reliable and sensitive and could be applied to predict the survival of patients with HNSCC (**Figure 7E**).

*Evaluation of the immunological characteristics and the therapeutics*

By analyzing the degree of infiltration of immune cells, we found that eosinophil and M0 macrophage were more abundant in the high-risk group, while B cell, M1 macrophage, M2 macrophage, mast cell, T cell regulatory, myeloid dendritic cell, CD4+ T cell and CD8+ T cell were more abundant in the low-risk group (**Figure 8A**). Most immune functions were statistically different between the high- and the low-risk groups except for the response to type I Interferon and major histocompatibility complex class I (**Figure 8B**). We also found that the expression of CTLA-4 ($P < 0.001$), PDCD1 ($P < 0.001$), LAG3 ($P < 0.01$), TIGIT ($P < 0.001$), BTLA ($P < 0.001$), and CD274 ($P < 0.05$) among others, was statistically different between the high- and the low-risk groups (**Figure 8C**).

The results of gene mutation analysis indicated that more genes were mutated in the high-risk group, and the top 20 genes with the highest frequency of alteration were shown in **Figure 9A** and **9B**. TIDE scores were lower in the high-

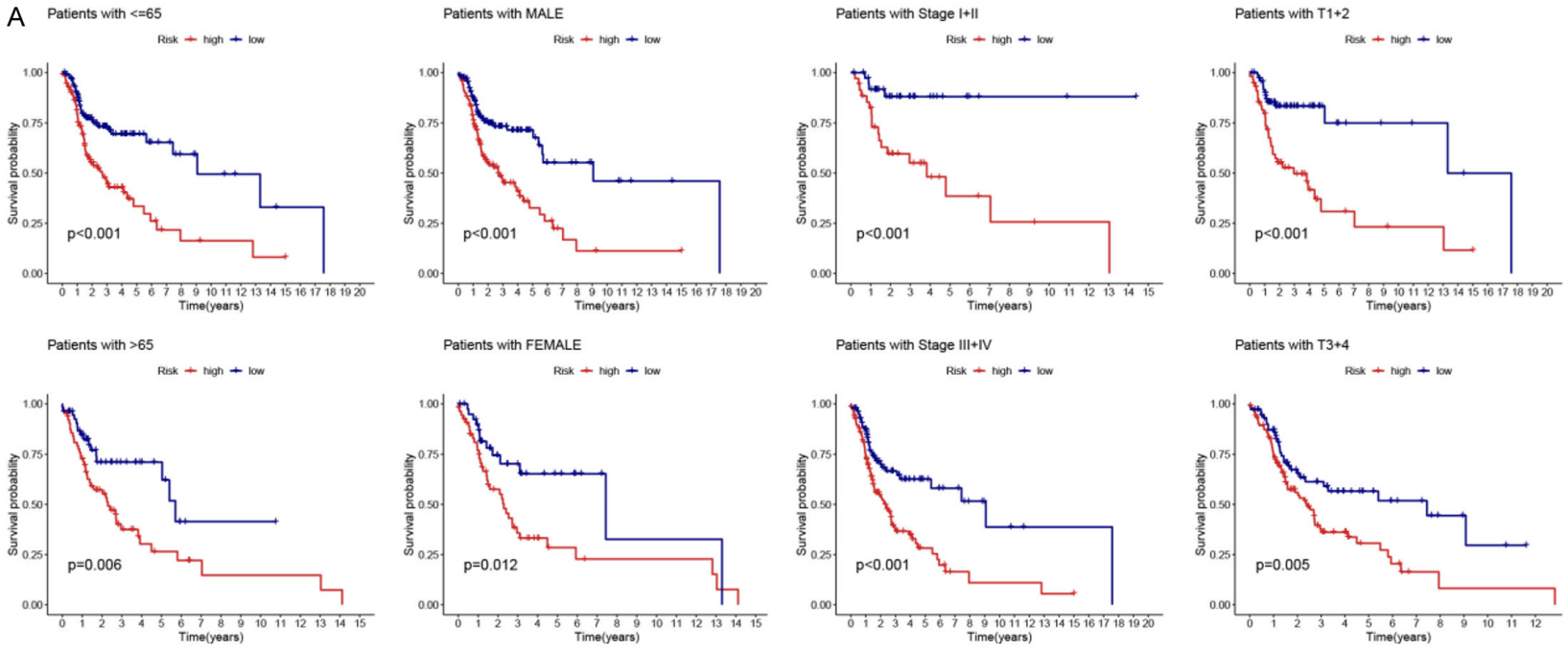
A
Patients with <=65
Risk high low
Survival probability
p<0.001
Time(years)
Patients with MALE
Risk high low
Survival probability
p<0.001
Time(years)
Patients with Stage I+II
Risk high low
Survival probability
p<0.001
Time(years)
Patients with T1+2
Risk high low
Survival probability
p<0.001
Time(years)
Patients with >65
Risk high low
Survival probability
p=0.006
Time(years)
Patients with FEMALE
Risk high low
Survival probability
p=0.012
Time(years)
Patients with Stage III+IV
Risk high low
Survival probability
p<0.001
Time(years)
Patients with T3+4
Risk high low
Survival probability
p=0.005
Time(years)

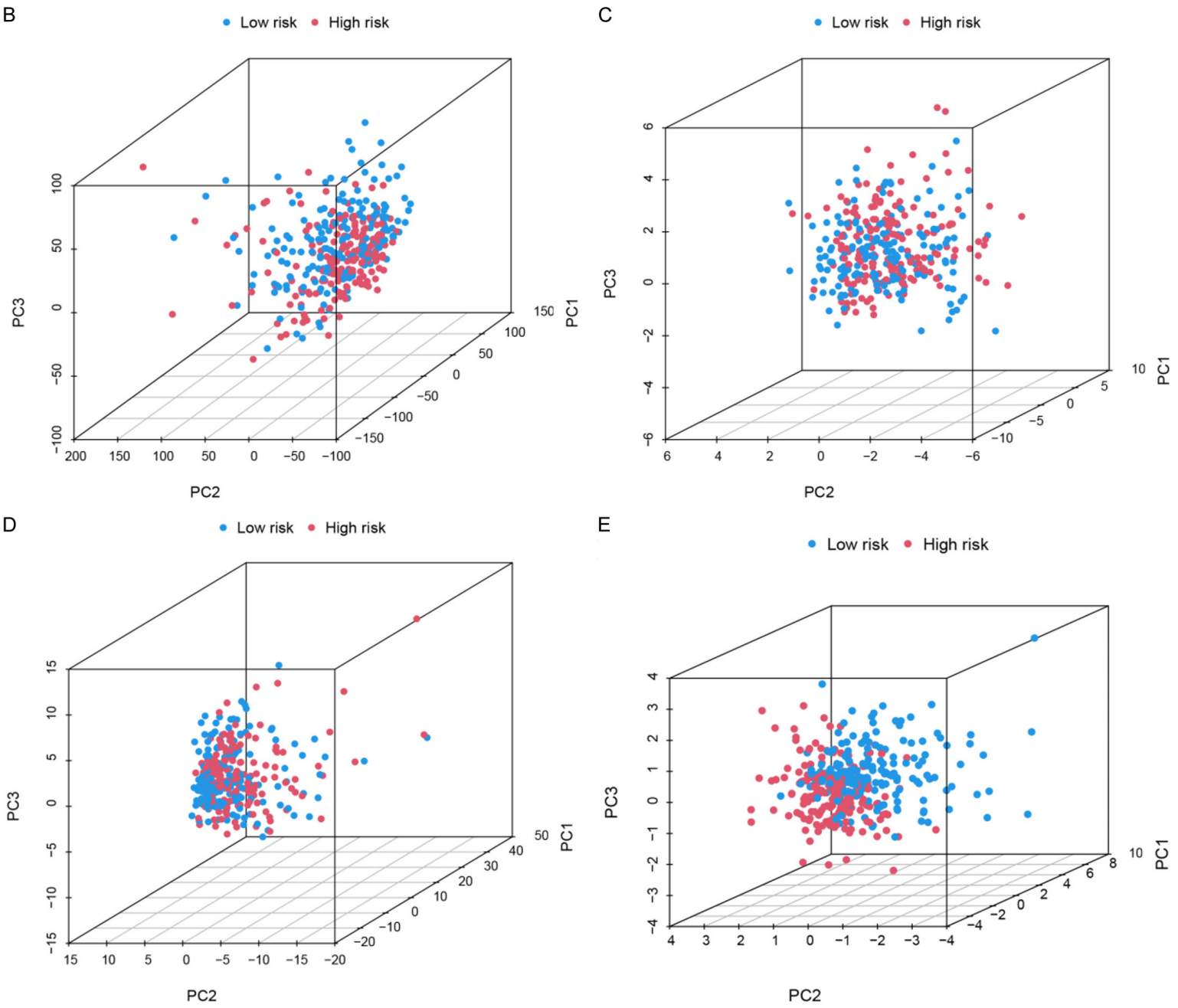
B
Low risk
High risk
PC3
PC2
PC1
C
Low risk
High risk
PC3
PC2
PC1
D
Low risk
High risk
PC3
PC2
PC1
E
Low risk
High risk
PC3
PC2
PC1

**Figure 6.** (A) In the subgroups defined by age, gender, pathological stage, and T stage, the patients in the low-risk group had longer survival times. (B-E) Principal component analysis (PCA) indicated that the distributions of whole gene expression profiles, 23 m$^6$A genes, and m$^6$AlncRNAs between different groups were relatively scattered (B-D), while the distributions of the nine m$^6$AlncRNAs in the signature between different groups had different distributions.

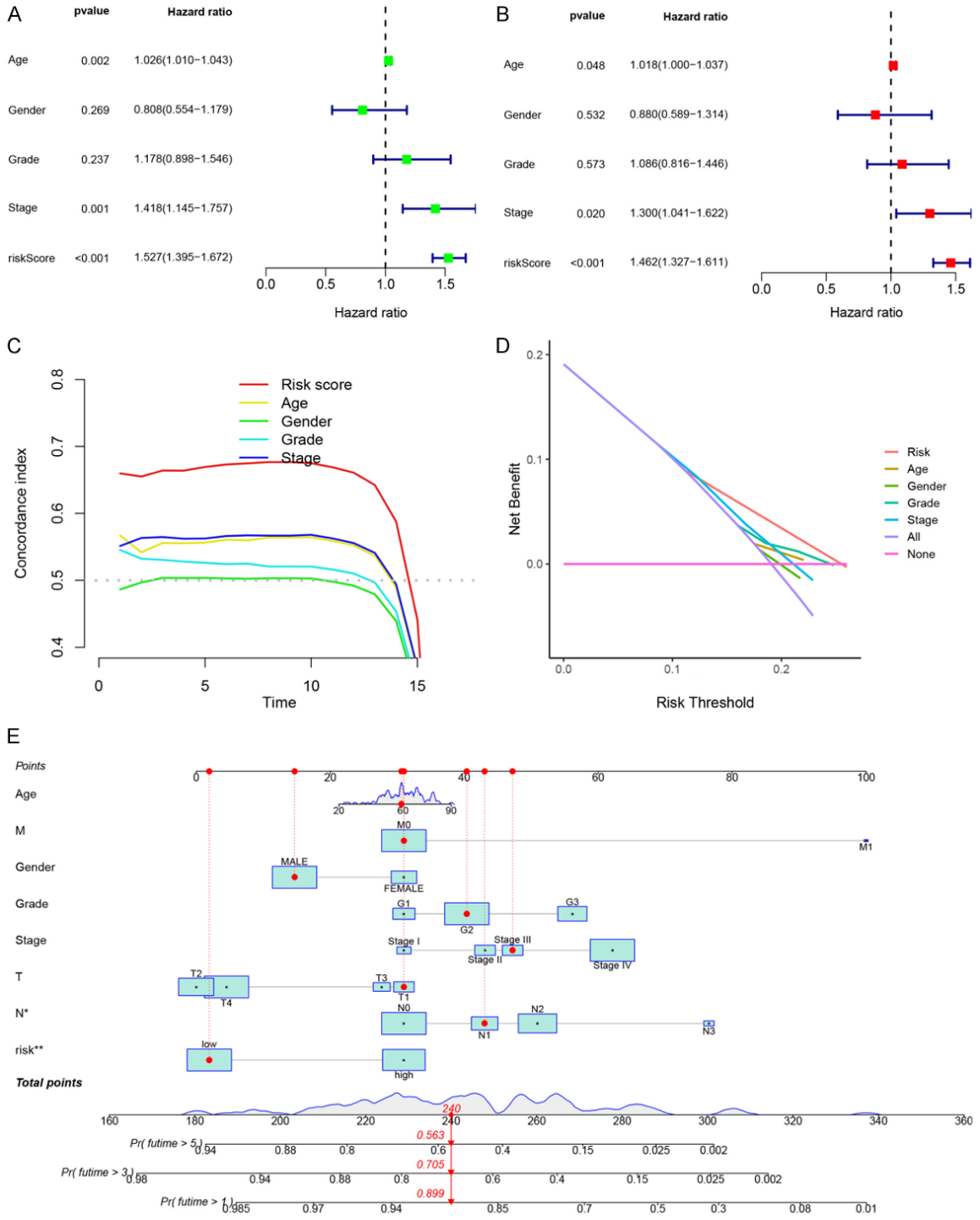


**Figure 7.** A, B. Univariate and multivariate Cox analysis demonstrated that risk score was an independent prognostic factor. C, D. The consistency index (C-index) and decision curve analysis (DCA) demonstrated that our model performed better in predicting the prognosis of HNSCC than other traditional clinical features. E. A nomogram based on clinical features and risk groups. *, P < 0.05; **, P < 0.01; ***, P < 0.001.

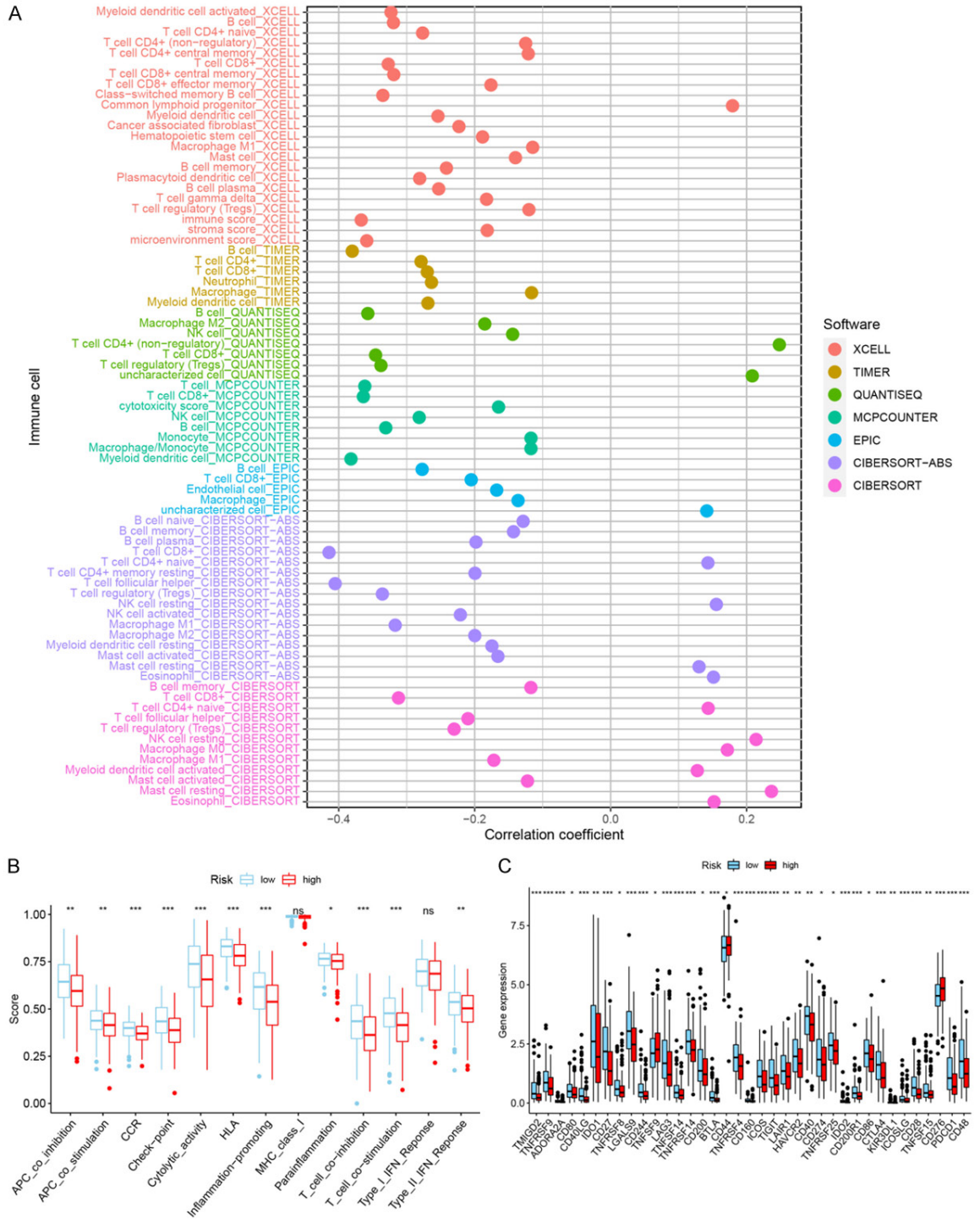


**Figure 8.** A. Estimation of tumor-infiltrating cells indicated that eosinophil and M0 macrophage were more abundant in the high-risk group, while B cell, M1 and M2 macrophage, mast cell, T cell regulatory, myeloid dendritic cell, CD4+ T cell and CD8+ T cell were more abundant in the low-risk group. B. The majority of immune functions were statistically different between different groups, except for response to type I Interferon and major histocompatibility complex class I. C. The expression of CTLA-4, PDCD1, LAG3, TIGIT, BTLA and CD274 was significantly different between different groups. *, P < 0.05; **, P < 0.01; ***, P < 0.001.

risk group (P < 0.001, **Figure 9C**), while TMB scores were higher in the high-risk group (P < 0.001, **Figure 9D**), indicating that patients in the high-risk group were more likely to be more

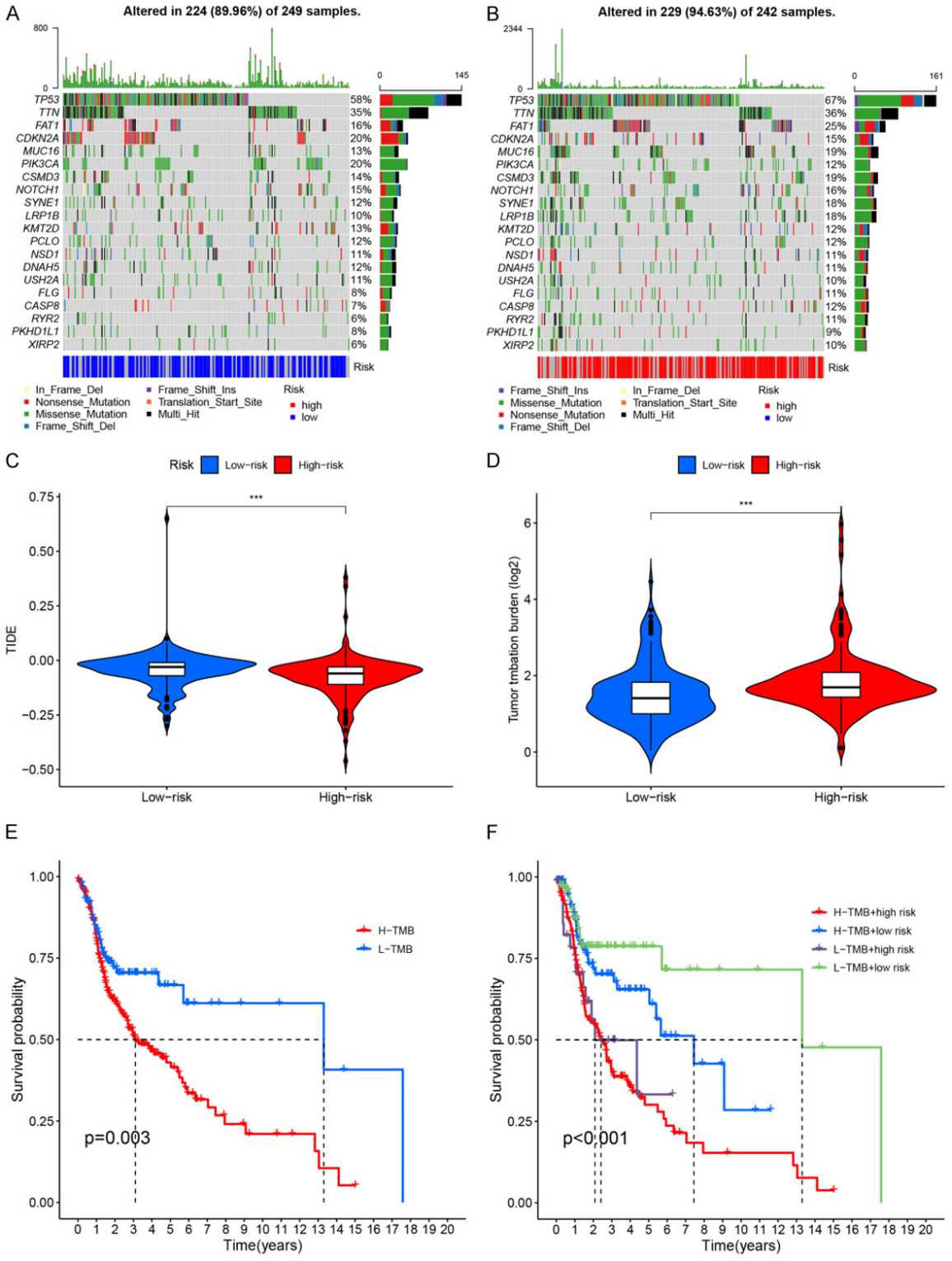


**Figure 9.** A, B. Gene mutation analysis displayed that more genes were mutated in the high-risk group. C. Tumor immune dysfunction and exclusion (TIDE) scores were lower in the high-risk group. D. Tumor mutational burden (TMB) scores were higher in the high-risk group. E. Survival rates were significantly lower in high-TMB groups. F. Survival rates were significantly different between four groups. *, P < 0.05; **, P < 0.01; ***, P < 0.001.

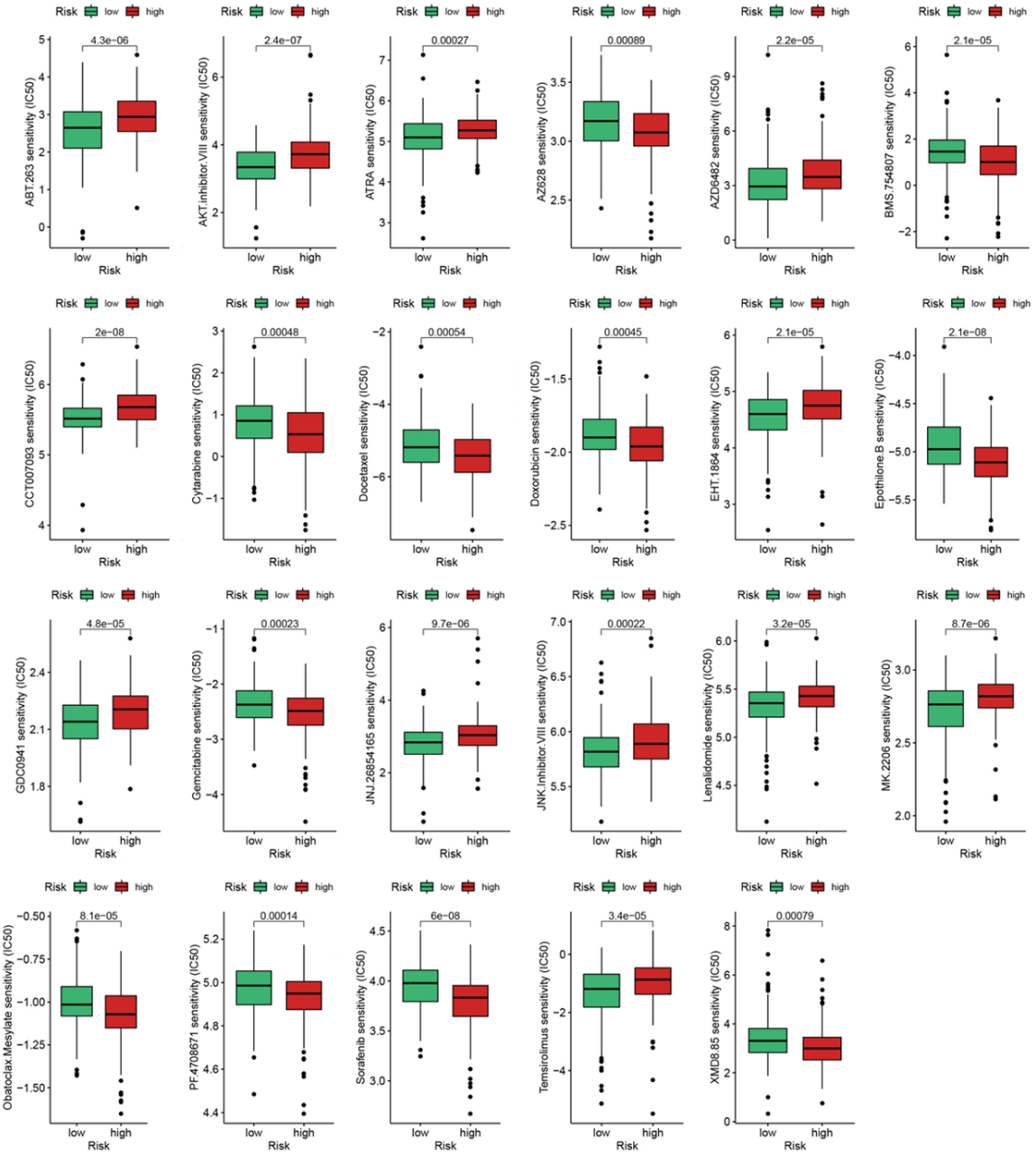


**Figure 10.** Identification of novel potential compounds for the treatment of HNSCC. P < 0.001.

sensitive to immunotherapy. Survival analysis revealed that the survival rates were statistically lower in high-TMB groups than in low-TMB groups (**Figure 9E**, P = 0.003), and **Figure 9F** showed the remarkable difference in survival rates among four groups (P < 0.001).

*Identification of novel potential compounds*

In addition to immunotherapy, we also sought to identify potential compounds targeting our signature for treating HNSCC patients. Based on the IC50, we identified several drugs that showed statistically differences in the IC50 between the high- and low-risk groups (**Figures 10**, S2).

## Discussion

In recent years, various studies have been carried out on the tumorigenesis, progression, and treatment of HNSCC [15]. Because of the het-

erogeneity of HNSCC, patients with comparable TNM stages may have distinct clinical characteristics and clinical outcomes [16]. Therefore, growing efforts have focused on constructing models with non-coding RNAs to predict the prognosis and the response to immunotherapy of HNSCC patients [16].

The m$^6$A is the most common form of modification in mammalian lncRNAs and has a broad impact on the structure and action of lncRNAs [20]. LncRNAs are the most abundant RNAs that play a significant role in various types of cancer through interactions with DNA, RNA, and proteins [20]. Studies have shown that m$^6$A could enhance the stability of lncRNAs to ensure their function, such as RNA-RNA interactions [22, 23]. The m$^6$A methylation modification of lncRNAs can affect different cellular activities in cancer cells [24]. Nevertheless, the research on the pathobiological effects of m$^6$A methylation of lncRNAs in HNSCC development is limited, and the potential therapeutic mechanisms and prognostic value of m$^6$AlncRNAs in HNSCC remain to be understood. Therefore, the current study sought to reveal the association between m$^6$A and lncRNAs and develop a risk model based on m$^6$AlncRNAs in HNSCC.

First, we identified 468 m$^6$AlncRNAs from the TCGA database, confirmed the prognostic potential of 35 m$^6$AlncRNAs, and constructed a model with 9 m$^6$AlncRNAs to predict the prognosis of HNSCC patients. Among the 9 m$^6$AlncRNAs we used, SNHG16 has been reported to regulate CCND1 expression by sponging miR-17-5p, thereby inhibiting the progression of oral squamous cell carcinoma [25]. Another study also showed that SNHG16 facilitated the cell proliferation and invasion of HNSCC by sponging miR-877-5p and up-regulating FOXP4 [26]. Another m$^6$AlncRNA identified in our study, JPX, was reported to play a crucial role in the proliferation, chemoresistance, anti-apoptosis, and aerobic glycolysis of glioblastoma by modulating the stability of PDK1 in an m$^6$A-dependent manner [27]. In addition, JPX accelerates HNSCC cell proliferation and migration by sponging miR-944 to up-regulate CDH2 [27]. Although SNHG16, JPX, and AL513190.1 have been identified as m$^6$AlncRNAs [13, 29], other m$^6$AlncRNAs were discovered for the first time.

Next, we assigned HNSCC patients into the high- and low-risk groups based on their median risk score, and the low-risk group had significantly better outcomes. We found that B cell, M1 and M2 macrophage, regulatory T cell, CD4+ T cell and CD8+ T cell were more abundant in the low-risk group. Interestingly, Distel et al. showed that B cell is a predictor of good prognosis in early HNSCC and negatively correlated with advanced HNSCC [13, 29]. Additionally, high infiltration of M1 macrophages and low infiltration of M2 macrophages are related to improved patient prognosis [31, 32]. However, in contrast to our findings, regulatory T cell has been described as a major contributor to the immune evasion and the poor prognosis in HNSCC [33]. On the other hand, CD4+ T cells and CD8+ T cells were reported to be the main anti-cancer cells and associated with the favorable prognosis in HNSCC, which was consistent with our findings [34, 35]. The discrepancy among different studies needs to be further clarified.

Recent studies have shown that the TIDE score can precisely predict the efficacy of immunotherapy [36]. Since we found TIDE scores were lower in the high-risk group, we predicted that the high-risk group was more likely to respond to immunotherapy. In addition, it has been reported that TMB can serve as an effective prognostic marker for predicting PD-L1 treatment response [37]. In our study, the TMB of the high-risk group was statistically higher, indicating that patients in the high-risk group probably benefit from anti-PD-1/PD-L1 monotherapy. Together, our predictive model could be a potential reliable biomarker for predicting the response to immunotherapy of HNSCC patients.

In clinical practice, TNM staging is a determinant of prognosis in HNSCC. However, HNSCC patients with similar TNM stages often have distinct clinical prognosis, indicating that the current TNM system fails to reflect the heterogeneity of HNSCC and is not a reliable prognostic marker. Thus, it is significant to identify novel biomarkers to predict the prognosis of HNSCC patients. We constructed the m$^6$AlncRNA signature to offer a new approach, and our findings provided insight into understanding the process and mechanism of the m$^6$A modification of lncRNAs. Nonetheless, the current study has several limitations. First, our sample size was relatively small, and the normal to tumor sample counts were not proportional. Second, the results might be biased

since the majority of samples from TCGA were non-metastatic. Third, our signature should be further validated by using external validation. Hence, we intend to expand the sample size and thoroughly follow up our results for our further prospective study.

In summary, the model we developed was accurate and efficient in predicting the prognosis of patients with HNSCC. Furthermore, our model could stratify HNSCC patients with good responses to immunotherapy. The findings from our study contributed to elucidating the processes and mechanisms of m$^6$AlncRNAs.

## Acknowledgements

We are appreciative of the TCGA database for providing these research-worthy data. This study was supported by the program of Southwest Medical University (2021ZKQN142).

## Disclosure of conflict of interest

None.

**Address correspondence to:** Drs. Sen Li and Wenjian Hu, The Affiliated Traditional Chinese Medicine Hospital of Southwest Medical University, No.182 Chunhui Road, Longmatan District, Luzhou 646000, Sichuan, China. E-mail: jht187@163.com (SL); huwenjian_7707@163.com (WJH)

## References

[1] Sung H, Ferlay J, Siegel RL, Laversanne M, Soerjomataram I, Jemal A and Bray F. Global cancer statistics 2020: GLOBOCAN estimates of incidence and mortality worldwide for 36 cancers in 185 countries. CA Cancer J Clin 2021; 71: 209-249.

[2] Leemans CR, Snijders PJF and Brakenhoff RH. The molecular landscape of head and neck cancer. Nat Rev Cancer 2018; 18: 269-282.

[3] Cramer JD, Burtness B, Le QT and Ferris RL. The changing therapeutic landscape of head and neck cancer. Nat Rev Clin Oncol 2019; 16: 669-683.

[4] Bozec A, Culié D, Poissonnet G and Dassonville O. Current role of primary surgical treatment in patients with head and neck squamous cell carcinoma. Curr Opin Oncol 2019; 31: 138-145.

[5] Yin J, Li X, Lv C, He X, Luo X, Li S and Hu W. Immune-related lncRNA signature for predicting the immune landscape of head and neck squamous cell carcinoma. Front Mol Biosci 2021; 8: 689224.

[6] Sun T, Wu R and Ming L. The role of m6A RNA methylation in cancer. Biomed Pharmacother 2019; 112: 108613.

[7] Yang Y, Hsu PJ, Chen YS and Yang YG. Dynamic transcriptomic mA decoration: writers, erasers, readers and functions in RNA metabolism. Cell Res 2018; 28: 616-624.

[8] Zhao BS, Roundtree IA and He C. Post-transcriptional gene regulation by mRNA modifications. Nat Rev Mol Cell Bio 2017; 18: 31-42.

[9] Ban Y, Tan P, Cai J, Li J, Hu M, Zhou Y, Mei Y, Tan Y, Li X, Zeng Z, Xiong W, Li G, Li X, Yi M and Xiang B. LNCAROD is stabilized by m6A methylation and promotes cancer progression via forming a ternary complex with HSPA1A and YBX1 in head and neck squamous cell carcinoma. Mol Oncol 2020; 14: 1282-1296.

[10] Li Y, Yan B, Wang X, Li Q, Kan X, Wang J, Sun Y, Wang P, Tian L and Liu M. ALKBH5-mediated m6A modification of lncRNA KCNQ1OT1 triggers the development of LSCC via upregulation of HOXA9. J Cell Mol Med 2022; 26: 385-398.

[11] Chen Y, Jiang X, Li X, Yan D, Liu J, Yang J and Yan S. The methylation modification of m6A regulators contributes to the prognosis of head and neck squamous cell carcinoma. Ann Transl Med 2021; 9: 1346.

[12] Deng Y, Li K, Tan F and Liu H. Gene model related to m6A predicts the prognostic effect of immune infiltration on head and neck squamous cell carcinoma. J Oncol 2021; 2021: 1-11.

[13] Feng ZY, Gao HY and Feng TD. Immune infiltrates of m$^6$A RNA methylation-related lncRNAs and identification of PD-L1 in patients with primary head and neck squamous cell carcinoma. Front Cell Dev Biol 2021; 9: 672248.

[14] Zhao X and Cui L. Development and validation of a mA RNA methylation regulators-based signature for predicting the prognosis of head and neck squamous cell carcinoma. Am J Cancer Res 2019; 9: 2156-2169.

[15] Chow L. Head and neck cancer. New Engl J Med 2020; 382: 60-72.

[16] Marur S and Forastiere AA. Head and neck squamous cell carcinoma: update on epidemiology, diagnosis, and treatment. Mayo Clin Proc 2016; 91: 386-396.

[17] Chen L, Cai Z, Lyu K, Cai Z and Lei W. A novel immune-related long non-coding RNA signature improves the prognosis prediction in the context of head and neck squamous cell carcinoma. Bioengineered 2021; 12: 2311-2325.

[18] Zheng J, Zhou Z, Qiu Y, Wang M, Yu H, Wu Z, Wang X and Jiang X. A prognostic ferroptosis-related lncRNAs signature associated with immune landscape and radiotherapy response in glioma. Front Cell Dev Biol 2021; 9: 675555.

[19] Zhou W, Pang Y, Yao Y and Qiao H. Development of a Ten-lncRNA signature prognostic model for breast cancer survival: a study with the TCGA database. Anal Cell Pathol 2020; 2020: 1-9.
[20] Wang JY and Lu AQ. The biological function of m6A reader YTHDF2 and its role in human disease. Cancer Cell Int 2021; 21: 109.
[21] Meng X, Wang ZF, Lou QY, Rankine AN, Zheng WX, Zhang ZH, Zhang L and Gu H. Long noncoding RNAs in head and neck squamous cell carcinoma: diagnostic biomarkers, targeted therapies, and prognostic roles. Eur J Pharmacol 2021; 902: 174114.
[22] Jin D, Guo J, Wu Y, Du J, Yang L, Wang X, Di W, Hu B, An J, Kong L, Pan L and Su G. MA mRNA methylation initiated by METTL3 directly promotes YAP translation and increases YAP activity by regulating the MALAT1-miR-1914-3p-YAP axis to induce NSCLC drug resistance and metastasis. J Hematol Oncol 2021; 14: 32.
[23] Yang D, Qiao J, Wang G, Lan Y, Li G, Guo X, Xi J, Ye D, Zhu S, Chen W, Jia W, Leng Y, Wan X and Kang J. N6-methyladenosine modification of lincRNA 1281 is critically required for mESC differentiation potential. Nucleic Acids Res 2018; 46: 3906-3920.
[24] Yi YC, Chen XY, Zhang J and Zhu JS. Novel insights into the interplay between m$^6$A modification and noncoding RNAs in cancer. Mol Cancer 2020; 19: 121.
[25] Wang Q, Han J, Xu P, Jian X, Huang X and Liu D. Silencing of LncRNA SNHG16 downregulates cyclin d1 (CCND1) to abrogate malignant phenotypes in oral squamous cell carcinoma (OSCC) through upregulating miR-17-5p. Cancer Manag Res 2021; 13: 1831-1841.
[26] Wang X, Liu L, Zhao W, Li Q, Wang G and Li H. LncRNA SNHG16 promotes the progression of laryngeal squamous cell carcinoma by mediating miR-877-5p/FOXP4 axis. Oncotargets Ther 2020; 13: 4569-4579.
[27] Li XD, Wang MJ, Zheng JL, Wu YH, Wang X and Jiang XB. Long noncoding RNA just proximal to X-inactive specific transcript facilitates aerobic glycolysis and temozolomide chemoresistance by promoting stability of PDK1 mRNA in an m6A-dependent manner in glioblastoma multiforme cells. Cancer Sci 2021; 112: 4543-4552.
[28] Yao Y, Chen S, Lu N, Yin Y and Liu Z. LncRNA JPX overexpressed in oral squamous cell carcinoma drives malignancy via miR-944/CDH2 axis. Oral Dis 2021; 27: 924-933.
[29] Zhang Y, Zhu B, He M, Cai Y, Ying X, Jiang C, Ji W and Zeng J. N6-methylandenosine-related lncRNAs predict prognosis and immunotherapy response in bladder cancer. Front Oncol 2021; 11: 710767.
[30] Distel LV, Fickenscher R, Dietel K, Hung A, Iro H, Zenk J, Nkenke E, Büttner M, Niedobitek G and Grabenbauer GG. Tumour infiltrating lymphocytes in squamous cell carcinoma of the oro- and hypopharynx: prognostic impact may depend on type of treatment and stage of disease. Oral Oncol 2009; 45: e167-e174.
[31] Alves AM, Diel LF and Lamers ML. Macrophages and prognosis of oral squamous cell carcinoma: a systematic review. J Oral Pathol Med 2018; 47: 460-467.
[32] Evrard D, Szturz P, Tijeras-Raballand A, Astorgues-Xerri L, Abitbol C, Paradis V, Raymond E, Albert S, Barry B and Faivre S. Macrophages in the microenvironment of head and neck cancer: potential targets for cancer therapy. Oral Oncol 2019; 88: 29-38.
[33] Stockis J, Roychoudhuri R and Halim T. Regulation of regulatory T cells in cancer. Immunology 2019; 157: 219-231.
[34] Borst J, Ahrends T, Bąbała N, Melief C and Kastenmüller W. CD4 T cell help in cancer immunology and immunotherapy. Nat Rev Immunol 2018; 18: 635-647.
[35] Farhood B, Najafi M and Mortezaee K. CD8 cytotoxic T lymphocytes in cancer immunotherapy: a review. J Cell Physiol 2019; 234: 8509-8521.
[36] Jiang P, Gu S, Pan D, Fu J, Sahu A, Hu X, Li Z, Traugh N, Bu X, Li B, Liu J, Freeman GJ, Brown MA, Wucherpfennig KW and Liu XS. Signatures of T cell dysfunction and exclusion predict cancer immunotherapy response. Nat Med 2018; 24: 1550-1558.
[37] Allgäuer M, Budczies J, Christopoulos P, Endris V, Lier A, Rempel E, Volckmar AL, Kirchner M, von Winterfeld M, Leichsenring J, Neumann O, Fröhling S, Penzel R, Thomas M, Schirmacher P and Stenzinger A. Implementing tumor mutational burden (TMB) analysis in routine diagnostics-a primer for molecular pathologists and clinicians. Transl Lung Cancer Res 2018; 7: 703-715.

**Table S1.** 23 m$^6$A-related genes

| Gene | Type |
|---|---|
| METTL3 | writers |
| METTL14 | writers |
| METTL16 | writers |
| WTAP | writers |
| VIRMA | writers |
| ZC3H13 | writers |
| RBM15 | writers |
| RBM15B | writers |
| YTHDC1 | readers |
| YTHDC2 | readers |
| YTHDF1 | readers |
| YTHDF2 | readers |
| YTHDF3 | readers |
| HNRNPC | readers |
| FMR1 | readers |
| LRPPRC | readers |
| HNRNPA2B1 | readers |
| IGFBP1 | readers |
| IGFBP2 | readers |
| IGFBP3 | readers |
| RBMX | readers |
| FTO | erasers |
| ALKBH5 | erasers |

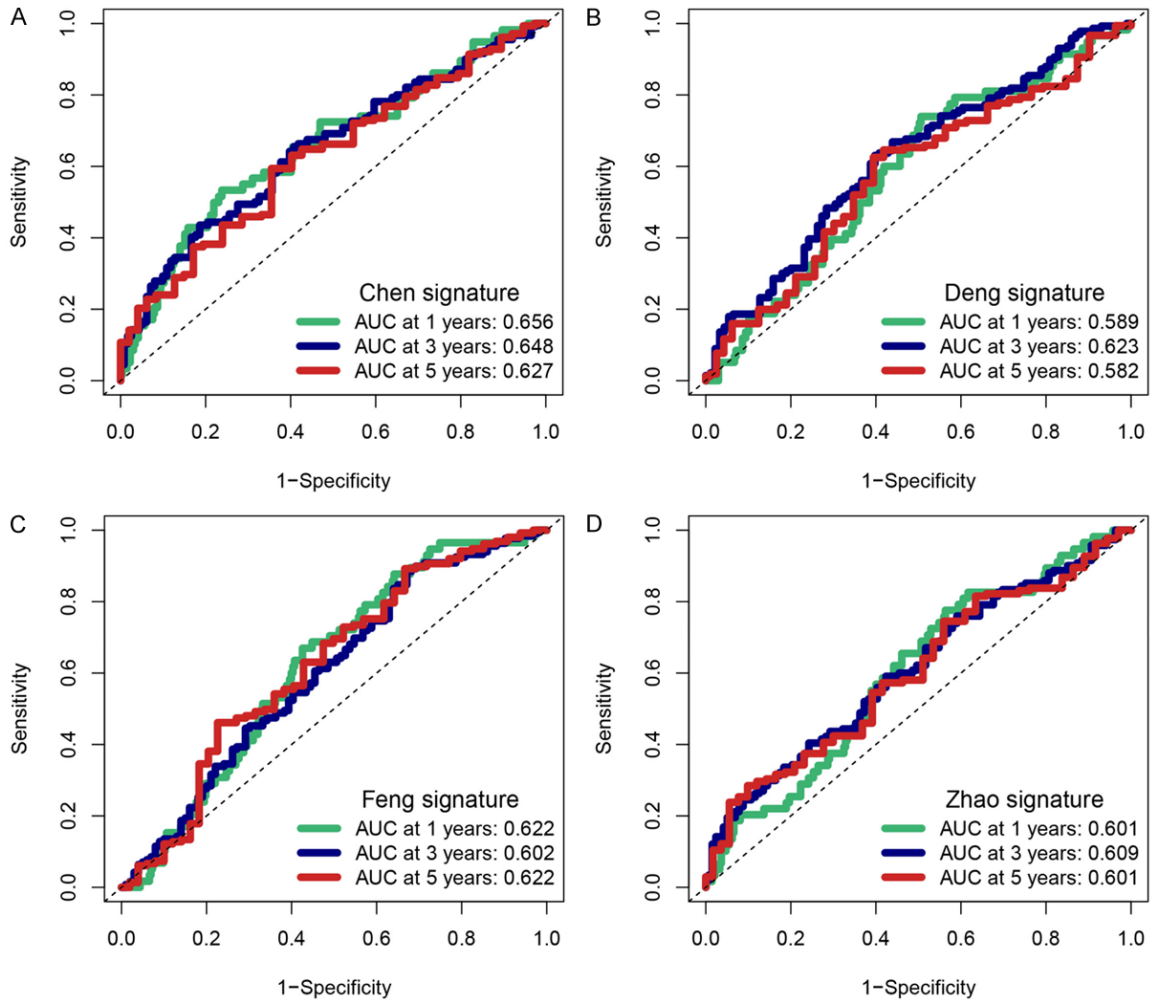


**Figure S1.** A-D. A comparison of 1, 3 and 5-year ROC curves with other established models indicated the superiority of this risk model.

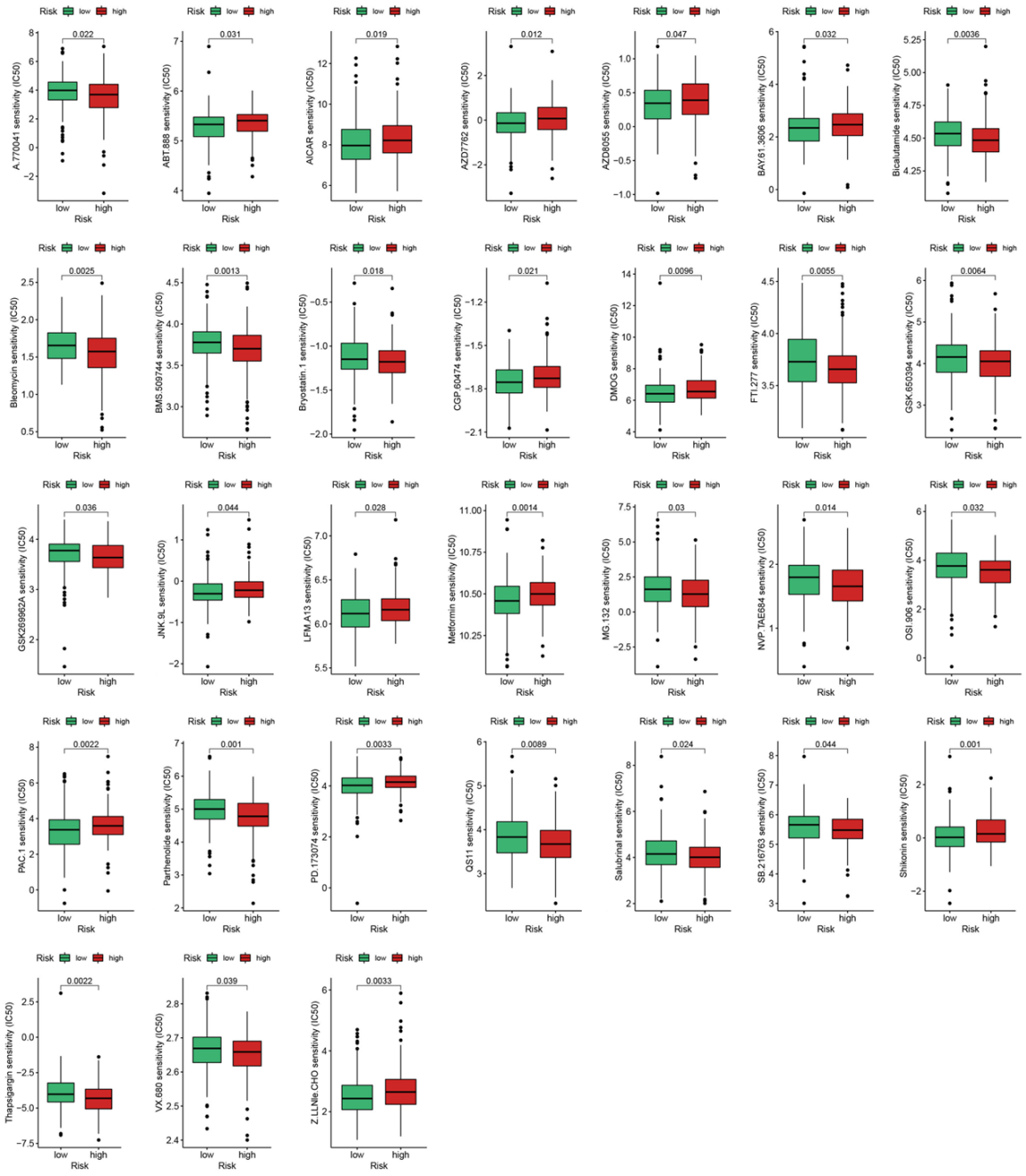


**Figure S2.** Identification of novel potential compounds targeting the model. P < 0.05.